



Mechanism and Prediction of Geothermal Resources Controlled by Neotectonics in Mountainous Areas: A Case Study of Southeastern Zhangjiakou City, China

Wenzhen Yuan¹, Xiaodong Lei², Tongzhe Liu³, Siqi Wang¹, Yifei Xing¹, Ruijie Zhu⁴, Fengtian Yang^{4*}, Dailei Zhang^{1*}, Jun Gao¹ and Baojian Zhang¹

¹Chinese Academy of Geological Sciences, Beijing, China, ²Beijing Institute of Geologic Survey Technology, Beijing, China, ³Institute of Hydrogeology and Engineering Geology, Shandong Provincial Bureau of Geology and Mineral Resources, Jinan, China, ⁴Key Laboratory of Groundwater Resources and Environment (Jilin University), Ministry of Education, Changchun, China

OPEN ACCESS

Edited by:

Yanlong Kong,
Institute of Geology and Geophysics
(CAS), China

Reviewed by:

Yonghui Huang,
Institute of Geology and Geophysics
(CAS), China
Chuanqing Zhu,
China University of Petroleum, China

*Correspondence:

Dailei Zhang
zhangdailei89@163.com
Fengtian Yang
yangfengtian@jlu.edu.cn

Specialty section:

This article was submitted to
Economic Geology,
a section of the journal
Frontiers in Earth Science

Received: 30 September 2021

Accepted: 21 February 2022

Published: 08 April 2022

Citation:

Yuan W, Lei X, Liu T, Wang S, Xing Y, Zhu R, Yang F, Zhang D, Gao J and Zhang B (2022) Mechanism and Prediction of Geothermal Resources Controlled by Neotectonics in Mountainous Areas: A Case Study of Southeastern Zhangjiakou City, China. *Front. Earth Sci.* 10:787156. doi: 10.3389/feart.2022.787156

The geothermal resources in mountainous areas are usually controlled by neotectonic faults. To minimize the risk in site selection for geothermal drilling, the controlling mechanism must be identified. Based on the neotectonic control theory for geothermal resources, the occurrence of the geothermal resources in the mountainous area in southeastern Zhangjiakou city was investigated. The investigation was divided into three stages. Firstly, field investigation for neotectonics was carried out to characterize the kinematics and the stress state of the faults, including fault occurrences, tectonic stages, and paleostress analysis, and in total 19 neotectonic faults were confirmed. Based on Riedel shear model and present stress field, their conductivity for geothermal water was inferred; secondly, geophysical and geochemical surveys were applied to identify the stress state and characterize the occurrence of the potential water conductive faults. The results showed that the combined use of magnetotelluric sounding (MT), controllable source audio magnetotelluric sounding (CSAMT), and 2D seismologic survey is effective in delineating fault occurrence, strata distribution, and water conductivity within 1,000 m depth, while measurement of ²²²Rn activity in soil gas across the neotectonic faults is effective to investigate the groundwater conductivity of the faults, and all the neotectonic faults in the study area striking clockwise from N5°E to N25°W are considered to be water conductive; thus, the areas at the intersection zones of neotectonic faults in the basin in groundwater runoff and discharge regions are promising targets for geothermal exploration. This conceptual model was verified by the geothermal fields already discovered in the study area and proved to be reasonable, and then a potential drilling site was predicted and proved to be successful. It is suggested that this workflow for geothermal exploration is suitable for Zhangjiakou city and may also be applied to other mountainous areas.

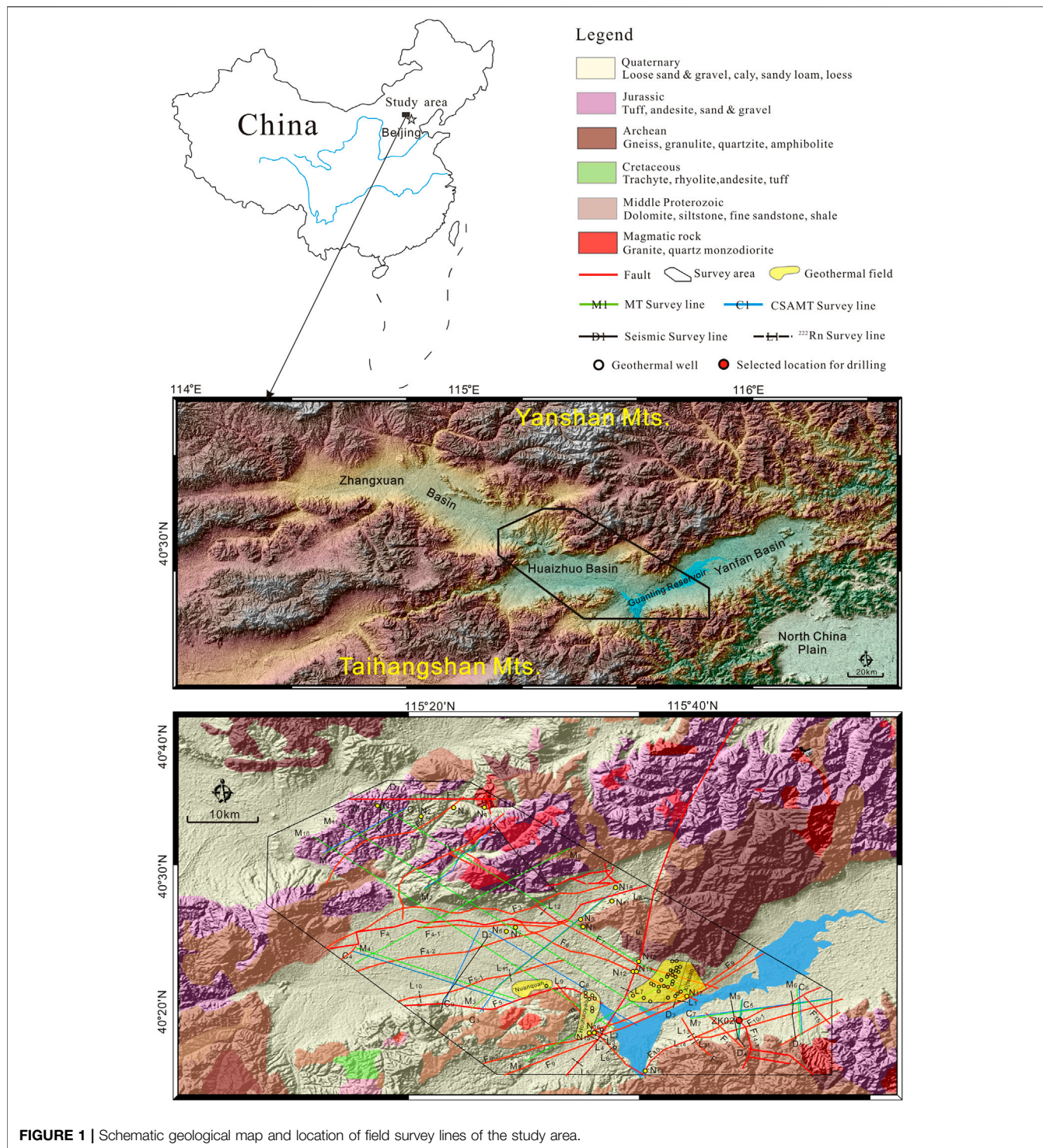
Keywords: neotectonic faults, geothermal resources, mountainous areas, conceptual model, drilling site prediction

INTRODUCTION

Hydrothermal resources are the main geothermal resources being used (Kong, 2017; Wang et al., 2017); accurate positioning of the resources is essential to reduce the overall development cost. Structurally, hydrothermal resources are distributed in large sedimentary basins and mountainous areas. Geothermal resources in sedimentary basins mainly occur in layered reservoirs and are easy to explore, whereas in mountainous areas are mainly controlled by open faults, and more investigation works are needed. Due to multi-stage structural evolution and complex structural features, it is often difficult to determine their mechanical properties through field observation. In addition, mechanical properties of faults are often segmented. These factors bring great risks to the prediction of geothermal resources targets. At present, the combination of geophysical and geochemical surveys is frequently applied to geothermal exploration in mountainous areas (Moghaddam et al., 2016). The geophysical methods adopted mainly include gravity, seismic and magnetotelluric surveys, etc. (Peng et al., 2019; Foley et al., 2020; Sena-Lozoya et al., 2020), while geochemical methods usually include soil gas (radon, CO₂, etc.) measurement, soil element geochemistry and hydrogeochemistry, etc. (Gang et al., 2012; Vaselli et al., 2013; Chang et al., 2014; Hanson et al., 2014; Pinti et al., 2017; Kong et al., 2020; Rodriguez et al., 2021). However, the application of these methods, such as survey line layout and data interpretation, must be based on the study of geological structures, especially on the understanding of how fault systems control the flow pathway of the thermal water; otherwise, it may result in blindness or great uncertainty in geothermal exploration. In the practice of geothermal exploration, there are many failed cases which resulted from ignoring the fact that the occurrence of thermal water in mountainous areas is controlled by open faults. Thus, it is key to identify the mechanical properties of the faults. In China, a theory named “Neotectonic control theory for geothermal resources” was proposed for convective hydrothermal resources (Xiao, 1986; Wang et al., 1993). The theory holds that whether a fault is open or closed depends on two most vital factors, i.e., its age and stress state. Generally, faults active in the Cenozoic are young enough and can hardly be infilled or cemented completely; thus, if the faults are tensile in the present stress field, they have the potential to act as a flow pathway for thermal water, and the area around the intersection zone of the tensile faults with other tensile or compressive shear faults in the regional groundwater discharge area would be the most promising area of hydrothermal resources. In this sense, faults active in the Cenozoic are regarded as neotectonic faults. Therefore, in the exploration of geothermal resources in the mountainous area, investigation and analysis of neotectonic faults should be firstly conducted to preliminarily infer their mechanical properties, followed by geophysical and geochemical surveys to identify if the faults are open, and then confirmed by drilling. Finally, the conceptual model of the thermal water controlled by neotectonic fault systems can be established, which would guide geothermal exploration.

Neotectonic faults have some distinctive characteristics; e.g., they are active in the Cenozoic, deep cutting, poorly infilled and cemented, and tensile (with high permeability) and thus control the formation of low to medium temperature convective type geothermal systems (Wang et al., 1993). Xiao (1986) summarized the characteristics of Cenozoic tectonic movement in China and proposed that neotectonic activities can be divided into four stages, namely, Paleogene, Neogene to the beginning of Quaternary, middle and late Quaternary, and Holocene. Here, according to the new tectonic stage division in China (Wan, 2011), the four stages are adjusted: the first stage is Paleocene (65–52 Ma), belonging to Sichuan Period; the second stage is Eocene to Oligocene, i.e., Huabei Period (52–23.5 Ma); the third period is Neogene to Early Pleistocene, i.e., Himalayan Period (23.5–0.78 Ma); and the fourth stage is the Middle Pleistocene to Holocene, that is, the Neotectonic Period (since 0.78 Ma). As tectonic stress fields in each period is different, the mechanical properties of the Neotectonic faults also change through the geological history. In field investigations, the mechanical properties and degree of openness of neotectonic faults can be preliminarily judged according to the characteristics of the pre-Cenozoic old structures and Neotectonic stress fields, the strike direction and mechanical properties of the faults formed under the Cenozoic tectonic stress fields, the history of neotectonic activities can be restored in combination with fault dating, and the openness of Neotectonic faults can be verified by means of geophysical and geochemical surveys. The Neotectonic control theory for geothermal resources has been widely applied in geothermal exploration practices to both low to medium and high temperature systems in China for approximately 30 years and has been verified to be effective (Yang et al., 2012; Lang et al., 2016; Kang et al., 2020). Zhangjiakou city is located in the northwest of Hebei Province, to the northwest of Beijing. It is an important node on the economic corridor between China, Mongolia, and Russia and is one of the new energy bases in national planning. In total, more than 20 geothermal fields have been found in this area, indicating a promising reserve of geothermal resources. In the mountainous region adjacent to Beijing in southeastern Zhangjiakou City, two large geothermal fields, i.e., Houhaoyao and Xijiabao, and one geothermal anomaly area, i.e., Nuanquan, have been found in recent years (**Figure 1**), but the genesis mechanism of the geothermal systems in this area is still not fully studied. Researchers believe that the geothermal anomaly in this area is related to the fracture network of deep faults but did not determine the mechanical properties of the faults due to limited field data and exploration depth (Wei, 2006; Li et al., 2020).

Based on previous researches and guided by the neotectonic control theory for geothermal resources, combined with geophysical and geochemical exploration methods, this research investigated and analyzed the mechanical properties of the neotectonic controlling faults, obtained the conceptual genesis model of the geothermal systems, then predicted the promising targets, and finally verified the geothermal potential by geothermal drilling. This study provides a reference for geothermal exploration in mountainous areas.



STUDY AREA

Local Geology

The study area is in the mountainous area in Northwest Hebei, to the northwest of Beijing. Tectonically, it includes the east of Zhangxuan Basin, the west of Huaizhuo Basin, and Yanfan Basin (Figure 1). The geomorphic units mainly include river

plains, hills, and mountains. The middle and low mountain areas are mostly tectonic erosion landforms dominated by carbonate rocks or igneous rocks. The terrain in the area fluctuates greatly; it is generally high in the northwest and low in the southeast. The altitude is between approximately 900 and 1,700 m, and the relative height difference is approximately 500–1,000 m.

The study area is a semi-arid area and has a temperate continental monsoon climate with four distinct seasons. The annual average temperature is 8°C. In hottest July, the average temperature is 24°C. The coldest month is January, and the average temperature is -9°C. The average annual precipitation is 360 mm, whereas the evaporation is 1,900 mm. The main rivers in the area belong to Yongdinghe River system of Haihe River Basin, which flows into the Guanting Reservoir, which is an important drinking water source for Beijing.

The strata in the study area comprise Archaean to Cenozoic except for the Lower Paleozoic, Upper Ordovician, Upper Paleozoic Silurian, Devonian, Carboniferous, and Permian. The Archean constitutes the regional basement, which is a set of metamorphic rock series formed under middle to deep regional metamorphism. The lithology is anorthosite, anorthosite amphibolite, and anorthosite gneiss. The Middle Proterozoic includes three systems, the Lower mainly consists of quartz sandstone, siltstone, sandy shale, etc., with carbonate lens at the bottom, and the strata thickness is 300–810 m. The Middle is dominated by carbonate rocks. The lithology is mainly dolomite and chert banded dolomite layered by quartz sandstone, siltstone, and shale. It outcrops in the northern mountainous areas north to the HuaiZhuo Basin, the thickness of dolomite is 370–1800 m, and the Upper system mainly comprises dolomite and quartz sandstone. The Paleozoic in the study area lacks Permian, Carboniferous, Devonian, Silurian, and Ordovician, and only the Cambrian outcrops sporadically. The Cambrian lithology is mainly Oolitic limestone, shale, argillaceous banded limestone, and marl. The formation thickness in this area is 230–400 m. The Triassic system is limited in distribution with a small thickness (approximately 70 m), which is mainly fluvial lacustrine sandy shale. The Jurassic is widely distributed throughout the region, which is composed of a set of complex continental volcanic sedimentary rock series. The main lithology is sandstone, conglomerate, tuff and andesite, etc. The Cretaceous comprises a set of river-lake facies, including terrigenous clastic rock and neutral volcanic rock strata distributed sporadically. The total thickness of the stratum reaches up to tens of thousands of meters. The Cenozoic includes Paleogene, Neogene, and Quaternary. The Paleogene includes Oligocene and Eocene, and the main lithology is basalt, interlayered with clay rock. The Neogene system in this area includes the Miocene and Pliocene. It is a set of river-lake facies and basic volcanic facies; the main lithology is interbedded sandy conglomerate and clay, which is not outcropped. Most of the study area is covered by the Quaternary, including Holocene (Q₄), Upper Pleistocene (Q₃), Middle Pleistocene (Q₂), and Lower Pleistocene (Q₁), and is mainly distributed in intermountain valleys and piedmont edges. It is a set of loose sand gravel, sandy soil, clay, and loess, with a general thickness of tens of meters, and reaches up to 150–700 m. At present, the distribution of strata in the area is mainly investigated based on the outcrops in surrounding mountainous areas. The detailed lithology and thickness of the formations in the study area are characterized by geophysical survey and drilling in this work.

The magmatism in the study area was intensive. It is a part of the Daxing'anling Mountain and Taihangshan Mountain tectonic magmatic belt. The major magmatic episodes occurred in the Mesozoic and reached the peak in the Middle and Late Mesozoic. The magmatic rock body formed is characterized by large scale, wide distribution and strong mineralization. It mainly occurs in the form of rock foundation, stock, wall, and branch in different scales. Magmatic intrusion and volcanic eruption are controlled by the Dahenan-Chicheng Fault (F₈), which strikes NE-NNE (**Figure 1**).

According to previous investigations, faults in the study area can be roughly divided into five groups, i.e., NW-, NWW-, ENE-, NNE-, and WE-striking faults, which are strike-slip faults. Some faults outcrop as normal or reverse faults at different segments, which is typical for wrench faults or a result of multi-stage activities. These faults have been described geometrically in previous studies, but the mechanical properties and permeability of the faults are still not fully studied, which is the focus of the present work.

Paleostress Regime

The study area has been folded and uplifted since the Jurassic and has experienced five main tectonic stages, accompanied by changes of stress fields, as a result of the tectonic regime transformation due to plate movement, i.e., the subduction of the North America Plate and Izanagi Plate to the west and northwest, respectively, in the Jurassic to Early Cretaceous, the fast northward movement of the Indian Plate and collision with the Eurasian Plate in the Middle Cretaceous-Paleogene, and the pushing against the Indian Plate and the Pacific Plate in the Eocene to Neotectonic. The principal stress of each tectonic stage is listed in **Table 1**. The faults in the study area generally show multi-stage activities in the Cenozoic under the paleostress regimes.

METHODOLOGY

The mechanical properties and water conductivity of the main faults in the study area are comprehensively investigated by 1) field investigation—according to the distribution of the main faults in the area, 10 routes are arranged for neotectonic investigation. The investigations include fault occurrences, tectonic stages, and paleostress analysis; 2) geophysical survey—three geophysical exploration methods were adopted, including magnetotelluric sounding (MT), controllable source audio magnetotelluric sounding (CSAMT), and two-dimensional (2D) seismology. The application of MT is to preliminarily find out the occurrence of faults and stratigraphic structure within 4,000 m depth, providing basis for further study on water conductivity of faults and reservoir structure. CSAMT is further applied to exploring the occurrence of the main faults within 1,500 m depth, inferring water conductivity of the faults, and lithology, burial depth, and thickness of reservoir and caprock in combination with geological and other geophysical data. Moreover, 2D seismology is applied to prospecting the occurrence of main faults and strata within 4,000 m depth in key

TABLE 1 | Tectonic stages and orientation of principal stress of the study area since Jurassic.

Geologic time	Tectonic periods	Orientation of principal stress
Jurassic to Early Cretaceous	Yanshan	NW-NNW (Wan, 2011)
Middle Cretaceous to Paleogene	Sichuan	NNE (Wan, 2003)
Eocene to Oligocene	Huabei	NWW (Wan, 2003)
Neogene to Early Pleistocene	Himalayan	NNW (Wan, 2003)
Middle Pleistocene to Holocene	Neotectonic	NEE ($80^\circ \pm 10^\circ$) (He, 1989)

TABLE 2 | Summary of field characteristics of the main faults in the study area.

Fault	Segment	Average strike	Stress state	Age	Type	^{222}Rn	MT and CSAMT	MT and 2D seismology
F1		WE	High tension	Q	Reverse		Impermeable	>1,000
F2–5	1	N40°E	Moderate tension	J	Normal		ND	>1,500
	2	N78°E	High tension	J	Normal		ND	>1,500
	3	N56°E	Moderate tension	J	Normal		ND	>1,500
F2–6	1	N6°W	Compression/shear	J	Normal		ND	>1,500
	2	N32°E	Low tension/weak shear	J	Normal		ND	>1,500
	3	N63°E	Moderate tension	J	Normal		ND	>1,500
	4	N48°E	Moderate tension	J	Normal		ND	>1,500
F3	1	N62°E	Moderate tension	Q	Reverse		Low conductive	2,000
	2	N87°W	High tension	Q	Reverse		Conductive	2,000–4,000
	3	N75°E	High tension	Q	Reverse		Conductive	4,000
F4		N84°E	High tension	Q	Normal		Conductive	>3,500
F4–1		WE	High tension	Q	Normal		Conductive	>3,500
F4–2		N78°E	High tension	Q	Normal		Conductive	>3,500
F5	1	N87°E	High tension	Q3	Normal		Conductive	1,300–5,000
	2	N82°W	Moderate tension	Q3	Normal		Conductive	1,300–5,000
	3	N71°E	High tension	Q3	Normal		Conductive	1,300–5,000
	4	N85°W	High tension	Q3	Normal		Conductive	1,300–5,000
	5	N75°W	Moderate tension	Q3	Normal		Conductive	1,300–5,000
F5–1		N76°E	High tension	Q3	Normal	Conductive	Conductive	1,300–5,000
F6		N67°W	Moderate tension	Q4	Normal		Conductive	4,000
F7	1	N60°W	Moderate tension	Q2	Normal	Conductive	Conductive	3,000
	2	N74°W	High tension	Q2	Normal	Conductive	Conductive	3,000
F8	1	N15°E	Low tension/weak shear	Q	Normal	Conductive	Conductive	>4,000
	2	N38°E	Moderate tension	Q	Normal	Conductive	Conductive	>4,000
	3	N26°E	Low tension/weak shear	Q	Normal	Conductive	Conductive	>4,000
F9		N65°E	High tension	Q2	Normal	Conductive	Conductive	>2,000
F9–1	1	N68°E	High tension	Q2	Normal	Conductive	Conductive	>2,000
	2	N55°E	Moderate tension	Q2	Normal	Conductive	Conductive	>2,000
F9–2		N75°E	High tension	Q2	Normal	Conductive	Conductive	>2,000
F10	1	N36°E	Moderate tension	Q3	Normal		Conductive	4,000
	2	N68°E	High tension	Q3	Normal		Conductive	4,000
F12		N40°W	Low tension/weak shear	Q	Normal	Conductive	Conductive	>3,000
F13	1	N31°W	Low tension/weak shear	Q	Normal	Conductive	Conductive	>3,000
	2	N50°W	Low tension/weak shear	Q	Normal	Low conductive	Conductive	>3,000
F14		N45°W	Low tension/weak shear	Q	Normal			
F15		N43°W	Low tension/weak shear	Q	Normal			

zones based on MT and CSAMT and conducting comprehensive interpretation of water conductivity of the main faults; and 3) soil gas survey— ^{222}Rn in soil gas is sensitive to water conductive faults and thus is a good indicator for the location of opened fault segments, where ^{222}Rn activity in soil gas would be much higher than further away from the faults. In this study, ^{222}Rn activity in soil gas was measured across the main fault segments along 15 profiles (Figure 1). ^{222}Rn activity was measured with a DURRIDGE RAD7 Radon Detector, with a precision of 10%.

The distance between two survey points is 50–200 m, and the measured depth is 0.8–1.1 m.

RESULTS AND DISCUSSION

Mapped Structures

Structural characteristics of the main faults were observed in the field at 18 outcrops; the field characteristics are summarized in

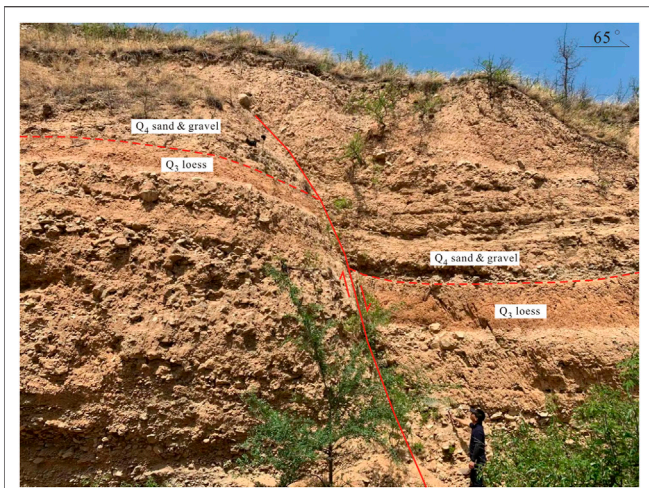


FIGURE 2 | ENE-striking normal fault (F_{10} , refer to **Figure 1**, N_{14} , for the location). The Late Pleistocene (Q_3) loess was cut by the fault, indicating the latest active age.

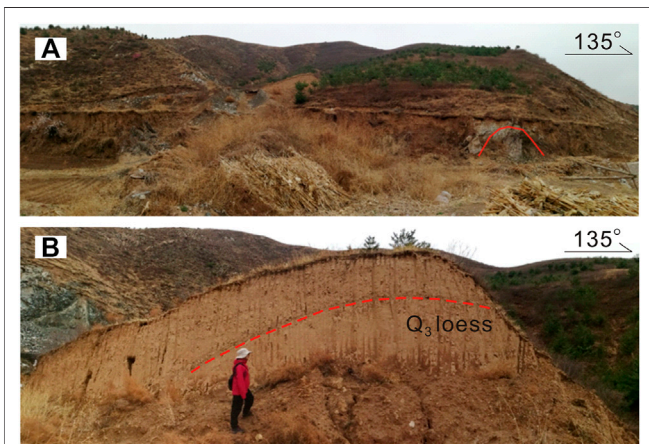


FIGURE 3 | NNE-striking normal fault and NW-striking fault (refer to **Figure 1**, N_{10} , for the location). **(A)** Panorama of the entire outcrop and an anticline developed in pre-Cenozoic formations. **(B)** Folded loess profile along the NW-striking fault, indicating the axis of compression in NW direction.

Table 2. The faults observed are mainly normal faults, and only a few ENE-striking (F_3) and WE-striking (F_1) faults are reverse faults. The latest active time of the faults found through field investigation is in Quaternary; thus, the main faults in the study area are neotectonic faults (**Figures 2, 3**) (Qi and Feng, 2019), except for F_{2-5} and F_{2-6} , which were developed in Jurassic, and no obvious signs of neotectonic activities were found. In total, 19 neotectonic faults were identified (**Table 2**).

Stress State of the Neotectonic Faults Under Present Stress

The regime of a stress field determines the type and orientation of faults generated, and subsequent changes of the stress field affect

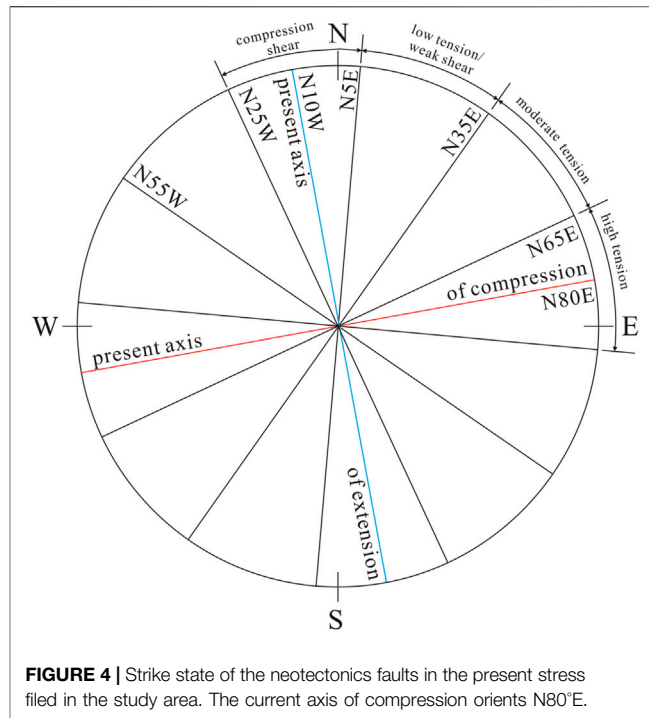


FIGURE 4 | Strike state of the neotectonic faults in the present stress field in the study area. The current axis of compression orients $N80^\circ E$.

the mechanical and hydrologic characteristics of the faults; thus, pre-existing faults may exhibit different hydrologic characteristics in the present stress field. The neotectonic faults would have developed heterogeneous hydrologic characteristics along strike due to local transtension or transpression (Dickerson and Fryer, 2009; Moore and Walsh, 2020). Therefore, the stress state of the neotectonic faults can be inferred by comparing the strike of the neotectonic faults and the orientation of the present stress field.

According to He (1989), the current axis of compression (greatest compressive stress) orients $N80^\circ \pm 10^\circ E$; thus, $N80^\circ E$ is adopted as the compromise value for all the data. According to Riedel shear model, assuming a typical angle of internal friction of 30° (Keaton, 2017), the maximum tension is interpreted to exist along any fault plane that is within 15° of $N80^\circ E$, which is normal to the axis of extension ($N5^\circ E$ to $N25^\circ W$), while the moderate tension is oriented within $15\text{--}45^\circ$ of the axis of compression ($N35^\circ E$ to $N65^\circ E$); the low tension with a component of weak shear stress is oriented within $15\text{--}45^\circ$ or parallel to the axis of extension (least compressive stress) ($N5^\circ E$ to $N25^\circ W$) and compression/shear within 15° or being parallel to the axis of extension ($N5^\circ E$ to $N25^\circ W$) (**Figure 4**) (Qi and Feng, 2019). Based on this model, the stress state of each fault segment was estimated (**Table 2**).

From the hydrogeologic point of view, the entire or certain segment of neotectonic faults could act as either pathways or barriers for groundwater flow depending upon their stress state. Neotectonic faults in tension would provide pathways, whereas faults in compression would act as planar barriers for groundwater flow (Xiao, 1986; Faut, 1997). According to the stress state of the neotectonic faults, water conductivity of the main faults in the area could be preliminarily judged. Except for the near NS-striking segment 1 of fault F_{2-6} , whose stress state is

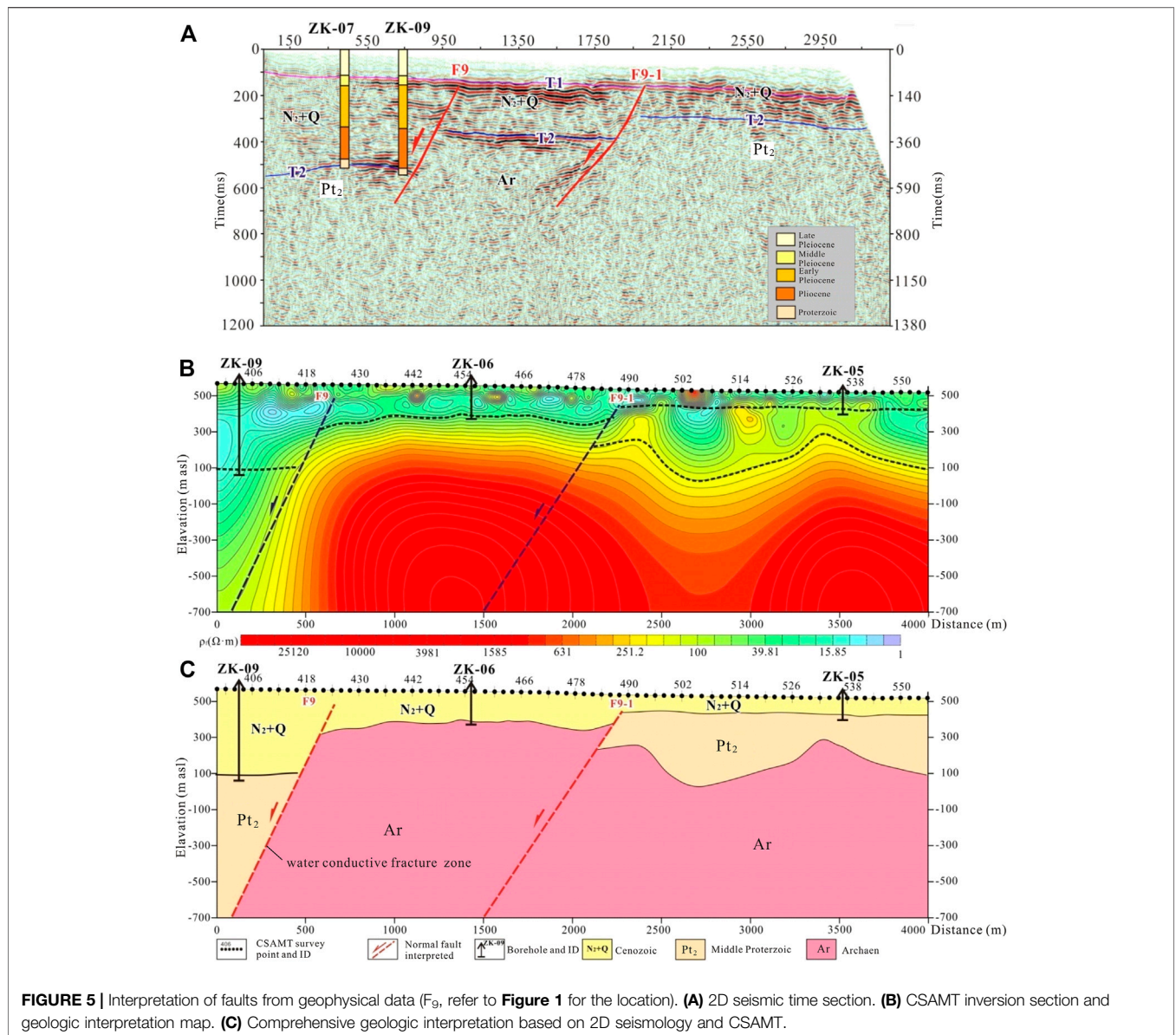


FIGURE 5 | Interpretation of faults from geophysical data (F₉, refer to Figure 1 for the location). **(A)** 2D seismic time section. **(B)** CSAMT inversion section and geologic interpretation map. **(C)** Comprehensive geologic interpretation based on 2D seismology and CSAMT.

compression/shear, and fault F1, which is a pre-Cenozoic fault and probably had been healed, the other faults are all neotectonic faults and in tension, having the potential to be pathways for thermal water. However, there are other factors affecting the potential, such as the intensity of current stress and paleostress, the scale of faults, etc. Therefore, water conductivity of the neotectonic faults should be further identified by both the geophysical and geochemical surveys.

Identification of Water Conductivity of Neotectonic Faults Geophysical Survey

Integral interpretation of geophysical data was conducted to delineate the occurrence of the neotectonic faults and evaluate their potential of being pathways for thermal water (Figure 5).

For MT and CSAMT data, faults were interpreted based on electrical discontinuity, which may result from displacement of strata on both sides of faults or accompanying fracture zone near faults, which facilitate the storage and flow of groundwater. As seismic reflection interface is a physical interface with different rock wave impedance, phase axis generally reflects underground lithologic interface. The main discrimination signs for faults are 1) reflected wave in-phase axis dislocation—due to different scale of faults, it may manifest as the dislocation of wave group and wave system of reflected waves. However, the wave group relationship on both sides of the fault is relatively stable, and the characteristics are clear, which is generally the reflection of medium and small-scale faults; 2) bifurcation, merging, distortion, and strong phase conversion occur in the standard reflection phase axis, which is generally a reflection of small-scale faults; 3) sudden increase/decrease or disappearance of reflection

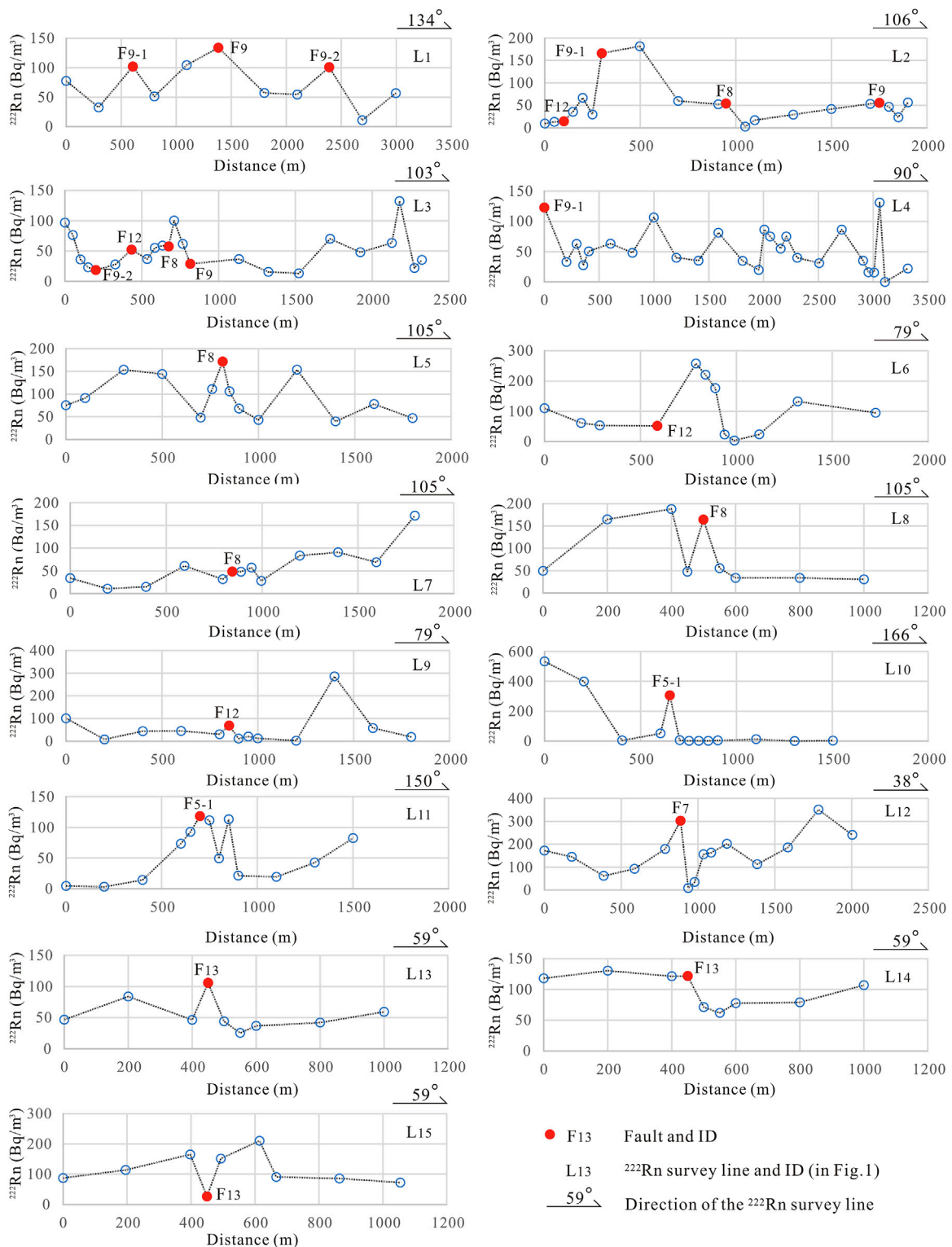


FIGURE 6 | ^{222}Rn activity in soil gas across main fault segments.

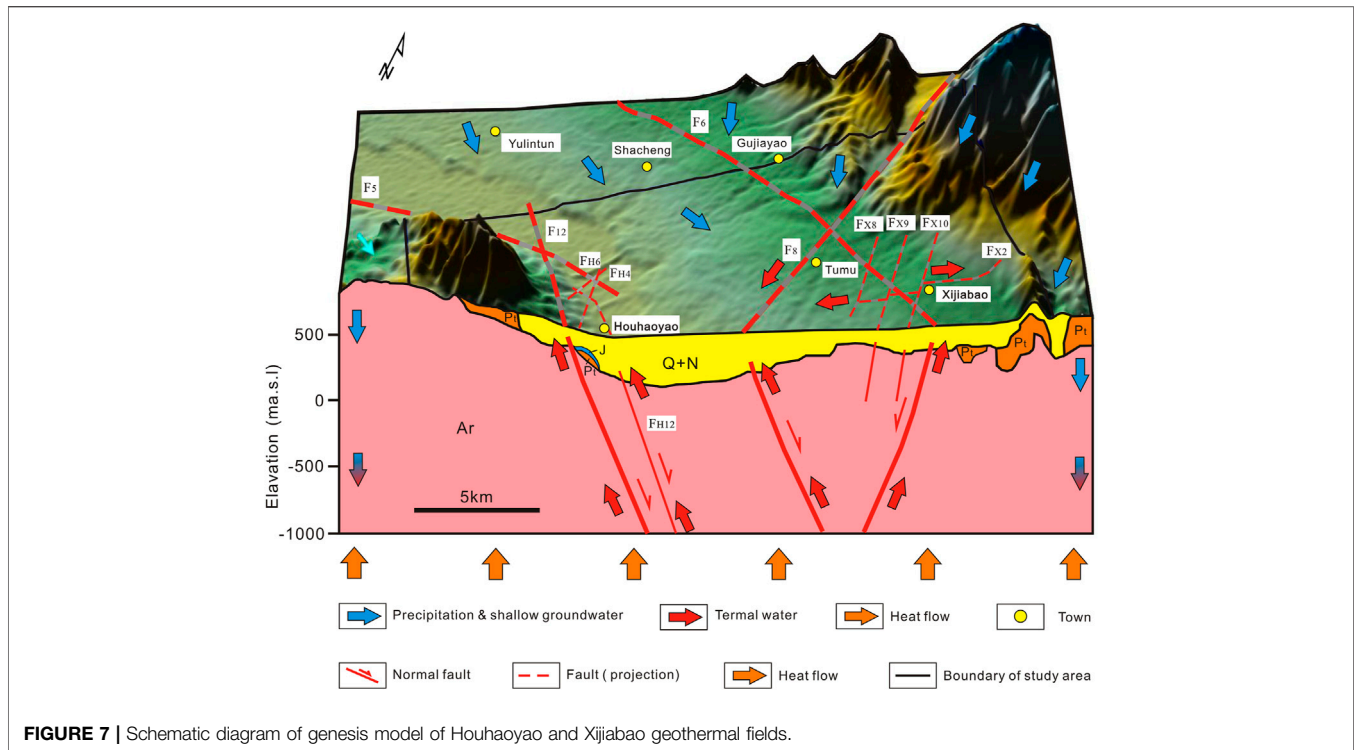


FIGURE 7 | Schematic diagram of genesis model of Houhaoyao and Xijiaobao geothermal fields.

phase axis or sudden change in wave group interval, which is often a reflection of large-scale faults; 4) abrupt changes in reflection phase axis, and the reflection is disordered or blank. This can be caused by strata displacement, sudden change of stratum occurrence on both sides, and distortion of reflected wave ray under fault plane due to shielding effect of fault; and 5) appearance of special waves, which is an important sign to identify faults, such as cross section wave and diffracted wave at the dislocation of reflection layer.

According to the interpretations based on geophysical surveys, most of the neotectonic faults have potential to be water conductive, except for fault F_1 , which is pre-Cenozoic and the water conductivity has probably diminished due to infill and cementation, and faults F_{2-5} and F_{2-6} , in which no significant large-scale continuous low resistance was found along the faults (Table 2). Some faults show heterogeneity in water conductivity in different segments, such as fault F_3 , in which the MT images (M_{10} , M_{11} , and M_{12} ; refer to Figure 1 for the location) show that low resistance in the southern segment of the fault is significant and extends to more than 4,000 m depth (segments 2 and 3), while in the northern segment (segment 1), the low resistance is weak and extends to only 2,000 m depth, indicating a lower permeability. This is consistent with the stress state of each segment of the fault; i.e., segment 1 is in moderate tension, whereas segments 2 and 3 are in high tension (Table 2).

Geochemical Survey

The water conductivity of the neotectonic faults is further reflected by ^{222}Rn activity in soil gas across main fault segments. ^{222}Rn activity in soil gas is influenced mainly by

faults permeability, groundwater table depth, lithology and physical properties of soil, and meteorological conditions including air moisture content, temperature, atmospheric pressure, and precipitation (Künze et al., 2012; Zarroca et al., 2012). Higher ^{222}Rn activity at the damage zone of the faults is interpreted as an indicator of good water conductivity. Results show that along the 15 survey lines, ^{222}Rn activities show significant heterogeneity across the faults (Figure 6). ^{222}Rn activities are usually higher at the fault zones than further from them, indicating that the faults are conductive for groundwater. The activities are above 50–100 Bq/m^3 , whereas further from the damage zone activities are lower. However, the ^{222}Rn activities also show significant differences for different faults or different segments of the same faults. For example, ^{222}Rn in soil gas is lower than 60 Bq/m^3 at F_{12} and lower than 125 Bq/m^3 at F_{13} but higher than 100 Bq/m^3 at F_9 and up to 306 Bq/m^3 at F_{5-1} . This could result from the difference in permeability of the faults due to different stress states; e.g., F_{12} and F_{13} are in low tension with weak shear, while F_9 and F_{5-1} are in high tension. For a certain fault, the ^{222}Rn along the fault also changes significantly, such as F_8 , where ^{222}Rn ranges from 48.5 to 171.6 Bq/m^3 within the fault zone from survey lines L_7 , L_2 , L_3 , and L_8 to L_5 ; F_9 , where ^{222}Rn activities range from 23.2 to 134.3 Bq/m^3 from survey lines L_3 and L_2 to L_1 ; F_{12} , where ^{222}Rn activities range from 14.7 to 69.1 Bq/m^3 from survey lines L_2 , L_3 , and L_6 to L_9 ; and F_{13} , where ^{222}Rn activities range from 26.4 to 121.7 Bq/m^3 from survey lines L_{15} and L_{13} to L_{14} . The heterogeneity in ^{222}Rn activities could result from differences in stress states of the fault segments, groundwater table depth, and permeability. For F_8 , the north part (segment 1) is in moderate tension and shows

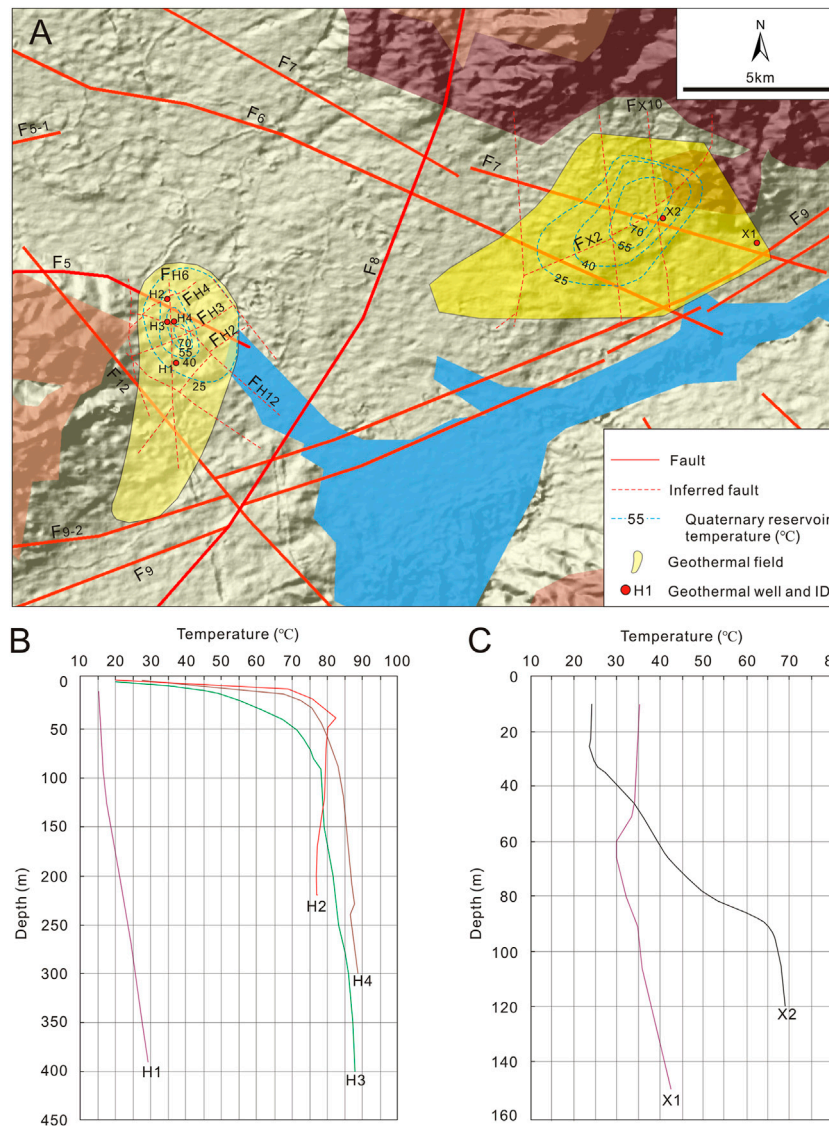


FIGURE 8 | (A) Location of Houhaoyao and Xijiabao geothermal fields. **(B, C)** Temperature–depth curve of geothermal wells in Houhaoyao and Xijiabao geothermal fields, respectively.

the highest ^{222}Rn activities (L_5), while the middle (segment 2) and south (segment 3) parts are in low tension with weak shear (Table 2), showing lower ^{222}Rn activities. Along these two parts, it is groundwater table depth which influences ^{222}Rn activities. In the mountainous area (L_8) with deeper groundwater table depth, ^{222}Rn activities are higher, whereas in the basin where groundwater table depth is shallower, the ^{222}Rn activities are lower (L_7 , L_2 , and L_3) (Figure 1). For F_9 , from L_1 to L_2 and L_3 along the groundwater flow direction, the ^{222}Rn activities decrease gradually as the groundwater table rises (Figure 1). For F_{12} , the ^{222}Rn activities also show a decreasing trend along the groundwater flow (from L_9 , L_6 , and L_3 to L_9). For F_{13} , the ^{222}Rn activities in the southeast segment (L_{15}) is significantly lower than that in the northwest segment (L_{13} and L_{14}) (Figure 1), indicating higher conductivity in the northwest segment. The highest ^{222}Rn

activities are at survey line L_{14} , where F_{10} and F_{13} intersect each other and the rocks are highly broken (Figure 1), resulting in a high permeability around the intersection zone. The ^{222}Rn activities are lower at L_{13} , reflecting the shallow depth of the groundwater table.

Case Study of Discovered Geothermal Fields

In order to check the water conductivity of the neotectonics faults, two discovered geothermal fields in the study area, i.e., Houhaoyao and Xijiapu geothermal fields, were chosen as study cases. These geothermal fields are located on the piedmonts of Huanzhuo Basin, where five regional faults, including F_5 , F_6 , F_7 , F_8 , F_9 , and F_{12} cross the region. The strata mainly comprise the Archean basement, Neogene and Quaternary, with limited distribution of the Jurassic and Middle Proterozoic. The

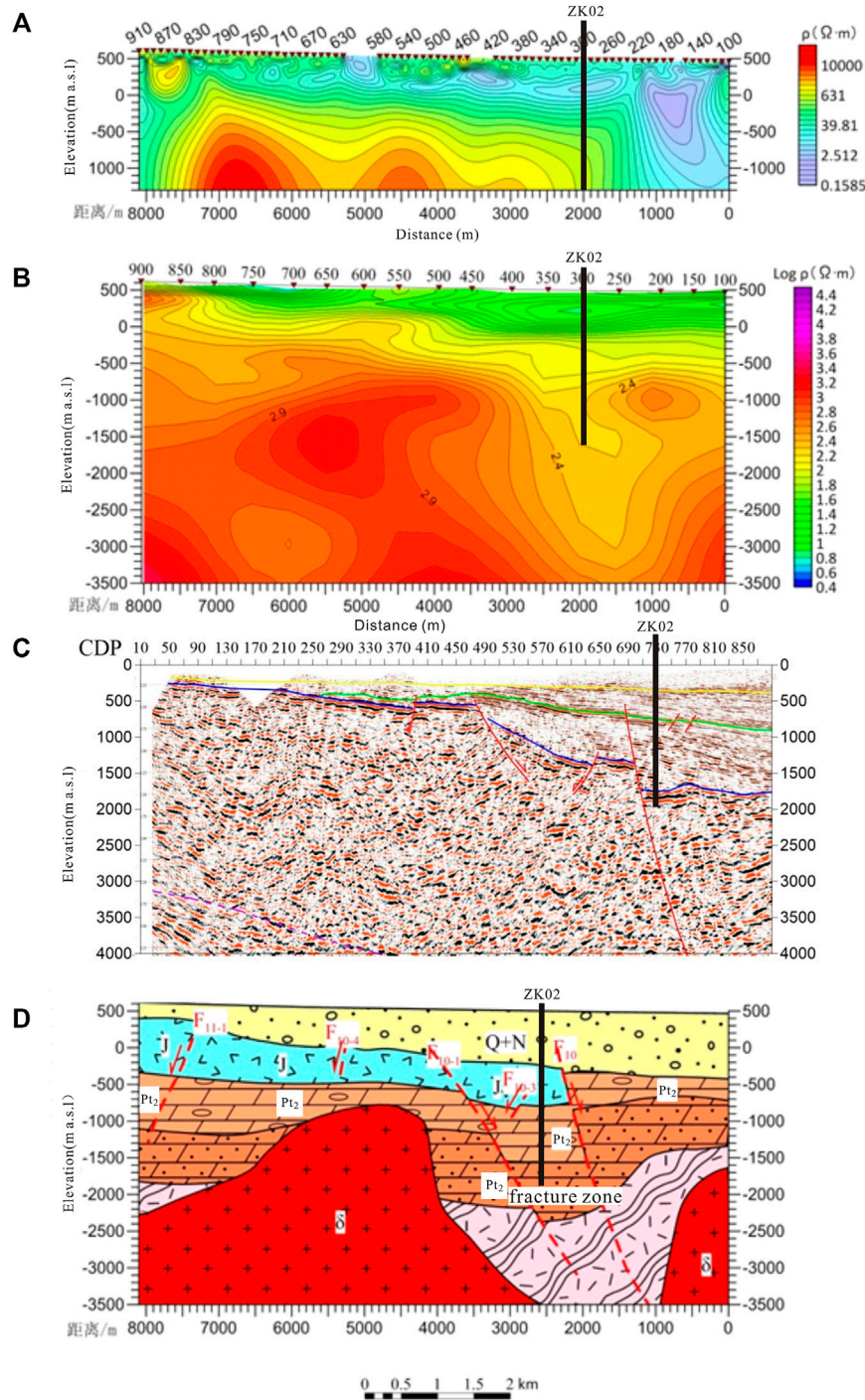


FIGURE 9 | Interpreted geologic profile of target Well ZK02. **(A)** Resistance inversion profile of C₅ survey line (refer to **Figure 1** for the location). **(B)** Resistance inversion profile of M₅ survey line (refer to **Figure 1** for the location). **(C)** Depth converted 2D seismic section of D₄ survey line (refer to **Figure 1** for the location). **(D)** Geologic interpretation map.

thickness of the Neogene and Quaternary is approximately 120–600 m and overlays the Archean directly (**Figure 7**). The Archean and the Neogene and Quaternary form a two-layer geothermal reservoir. The open neotectonic faults in the Archean constitutes the bedrock geothermal

reservoir, and as the thermal water flows up into the Neogene and Quaternary, the shallow sandstone reservoir forms. The temperature of the regional shallow groundwater is 10–15°C, while the well head temperature of the thermal water in these geothermal fields are usually 44.5–68.5°C, with the highest

temperature of 88.6°C. Assuming the 25°C-isothermal line of groundwater as the boundary of the geothermal reservoirs, the distribution of the reservoirs was determined (**Figure 8A**).

Geophysical surveys showed that there are many secondary or small-scale faults in the geothermal fields. According to MT and CSAMT, in Houhaoyao geothermal field, NE-striking faults F_{H2} , F_{H3} , and F_{H4} and NW-striking fault F_{H12} are normal faults and show low resistance in the deep, indicating that they are water conductive. The low resistance zones of F_{H2} , F_{H3} , and F_{H4} were found to be connected below approximately 3,000 m depth and were inferred to be secondary faults of F_8 . Fault F_{H6} has higher resistance in the deep, indicating a lower water conductivity. Well temperature loggings show that wells in the intersection zones of the F_5 , F_{H3} , F_{H4} , and F_{H6} show significant temperature anomaly; e.g., the temperature in Wells H_2 , H_3 , and H_4 increases sharply to 75–89°C from 30 m–400 m depth, whereas temperature anomalies in wells further from the intersection zones are weak; e.g., in Well H_1 near Fault F_{H6} , the well temperature increases slowly from 10°C to 29°C between 10 and 400 m depth (**Figure 8B**). In Xijiabao geothermal field, Fault F_{X2} shows low resistance from 400 m depth in the Quaternary; the fault is a normal fault with an offset of 200–300 m, indicating it is a water conductive neotectonics fault, while the NNW-striking faults F_{X8} , F_{X9} , and F_{X10} show no significant low resistance in the deep and were inferred as groundwater barriers. Groundwater in wells near the intersection zone of F_{X10} and F_{X2} shows the highest temperature; e.g., the well head temperature of Well X_2 increased quickly from 24°C to 70°C between 10 and 120 m depth, whereas the temperature in Well X_1 near the intersection zone of F_9 and F_7 increases slower from 35°C to 43°C between 10 and 150 m depth (**Figure 8C**), indicating the thermal water mainly flows up from F_{X2} . The water conductivity of the faults can also be reflected by the geometry of the isothermals of the groundwater; in the two geothermal fields, the long axis of the isothermals is controlled by the intersection zones of the NE-striking faults and the other faults, indicating the NE-striking faults are water conductive.

Thus, the circulation of the thermal water in these geothermal fields is controlled by open neotectonics faults striking NE and NW; where they are intersected by NNW-striking faults which are water barriers, or other water conductive faults, the stratum is broken, facilitating the upflow of thermal water (**Figure 7**).

PREDICTION AND VERIFICATION OF TARGET AREA

According to the analysis above, all the neotectonic faults in the study area striking clockwise from N5°E to N25°W are likely to be water conductive; the areas at the intersection zones of neotectonic faults in the basin in groundwater runoff and discharge regions are promising targets for geothermal

exploration. Based on this conceptual model, a potential site for geothermal drilling was selected in Donghuan Yuan Town, located southeast of the study area (**Figure 1**). Geophysical exploration revealed that the geothermal reservoir is a fracture zone in dolomite of the Middle Proterozoic; the burial depth of the reservoir is approximately 1,000 m, with a thickness of approximately 1,000 m. The caprock is Quaternary, Neogene, and Jurassic. There are several groups of intersecting faults and fracture zones in the area, which is favorable for enrichment of thermal water.

The proposed Well ZK02 is located at point 290 along C_5 survey line (**Figure 1**). The location was selected based on the following reasons: 1) the target area is located at the intersection of two groups of neotectonic faults striking NEE (F_{10}) and NNW (F_{14-1}); 2) on the gravity anomaly and aeromagnetic anomaly map (Yuan et al., 2021), the target area is located in the northwest of the northeast gradient zone; 3) the inverted resistance of C_5 survey line and M_5 survey line (**Figure 1**) changes greatly in the transverse direction, and there is an obvious low resistance zone which extends to approximately 3,000 m depth, indicating that the water yield of deep karst affected by the faults is excellent; and 4) the phase axis of D_4 survey line (**Figure 1**) is obviously broken at this point, indicating that layer T_2 is disconnected from the Middle Proterozoic, with an offset of approximately 500 m (**Figure 9**).

The strata encountered by drilling include the Quaternary and Neogene, with a bottom depth of 1,327.9 m, and the lithology is clay, sand, gravel, and glutenite; the Middle Proterozoic has a bottom depth of 2,960 m and a thickness of 1,632 m, and the lithology is mainly dolomite, shale, glutenite, and mudstone, containing diorite porphyrite veins; the bottom depth of the Archean is 3,006.9 m, the drilled thickness is 46.9 m, and the lithology is mainly granite gneiss.

The well is artesian after completion, with a static water level of 9.8 m above the ground. The well temperature measured 72 h after drilling at the depth of 3,000 m was 69.0°C. Results from three drawdown pumping tests show that when the drawdown is 34 m, the water yield reaches up to 160.4 m³/h, proven to be a high-quality geothermal well.

CONCLUSION

In total, 19 neotectonic faults were identified in a field neotectonic investigation in Yanfan and Xuanhuai Basins, among which the faults striking clockwise from N5°E to N25°W are tensile faults under the present stress field. The combined use of MT, CSAMT, and 2D seismologic survey was proved to be effective in delineating fault occurrence, strata distribution, and water conductivity.

Measurement of ²²²Rn activity in soil gas across neotectonic faults is useful to investigate the groundwater conductivity of the faults. The ²²²Rn activity is mainly influenced by stress state of the fault, groundwater table depth, and the rock broken degree.

The areas at the intersection of water conductive neotectonic faults located in groundwater runoff or discharge area are most promising for geothermal exploration. Based on the neotectonic control theory for geothermal resources and geophysical exploration, the location of geothermal Well ZK02 in Donghuanyuan Town is successfully selected, which is proved to be a high-quality geothermal well by drilling.

This study shows that the application of neotectonic control theory for geothermal water in geothermal resource exploration in Zhangjiakou mountainous area is effective and has the potential to be extended to other mountainous regions (Wang et al., 2015).

DATA AVAILABILITY STATEMENT

The original contributions presented in the study are included in the article; further inquiries can be directed to the corresponding authors.

REFERENCES

- Chang, Z. Y., Shi, J., Li, Q. H., Zhao, H. B., and Zhou, X. Y. (2014). The Application of Soil Radon Measurement Technology to Geothermal Exploration in Taxkorgan County, Xinjiang. *Geophys. geochemical exploration* 38 (4), 654–659. doi:10.11720/wtyht.2014.4.05
- Dickerson, R., and Fryer, W. (2009). “Potential Effects of Faults on Groundwater Flow for the Yucca Flat Basin, Nevada Test Site,” in *American Geophysical Union, Fall Meeting 2009, Abstract ID, H33B-H0874*.
- Foley, N., Tulaczyk, S., Auken, E., Grombacher, D., Mikucki, J., Foged, N., et al. (2020). Mapping Geothermal Heat Flux Using Permafrost Thickness Constrained by Airborne Electromagnetic Surveys on the Western Coast of Ross Island, Antarctica. *Exploration Geophys.* 51 (1), 84–93. doi:10.1080/08123985.2019.1651618
- Gang, F. P., Lyv, Y., Yu, L. P., and Chen, Y. X. (2012). The Utilization of Combined Radon and CSAMT Methods to Detect Underground Geological Structures: a Case Study of Detection in Palian and Fapa Profiles, Luxi Area, Western Yunnan Province. *Geol. Bull. China* 31 (Z1), 389–395. doi:10.3969/j.issn.1671-2552.2012.02.024
- Hanson, M. C., Oze, C., and Horton, T. W. (2014). Identifying Blind Geothermal Systems with Soil CO₂ Surveys. *Appl. Geochem.* 50, 106–114. doi:10.1016/j.apgeochem.2014.08.009
- He, S. H. (1989). Calculation of the Affections of the Principal Stress Direction and Magnitude on the Fault Reactivation. *Crustal Deformation and Earthquake* 9 (3), 44–52.
- Kang, F. X., Sui, H. B., and Zheng, T. T. (2020). Heat Accumulation and Water Enrichment Mechanics of piedmont Karstic Geothermal Reservoirs: a Case Study of Northern Jinan. *Acta Geologica Sinica* 94 (5), 1606–1624. doi:10.19762/j.cnki.dizhixuebao.2020150
- Keaton, J. R. (2017). “Angle of Internal Friction,” in *Encyclopedia of Engineering Geology. Encyclopedia of Earth Sciences Series*. Editors P. Bobrowsky, and B. Marker (Cham: Springer). doi:10.1007/978-3-319-12127-7_16-1
- Kong, Y., Pang, Z., Pang, J., Li, J., Lyu, M., and Pan, S. (2020). Fault-Affected Fluid Circulation Revealed by Hydrochemistry and Isotopes in a Large-Scale Utilized Geothermal Reservoir. *Geofluids* 2020, 1–13. doi:10.1155/2020/2604025
- Kong, Y., Pang, Z., Shao, H., and Kolditz, O. (2017). Optimization of Well-Doublet Placement in Geothermal Reservoirs Using Numerical Simulation and Economic Analysis. *Environ. Earth Sci.* 76, 118. doi:10.1007/s12665-017-6404-4
- Künze, N., Koroleva, M., and Reuther, C. D. (2012). ²²²Rn Activity in Soil Gas across Selected Fault Segments in the Cantabrian Mountains, NW Spain. *Radiat. Measurements* 47 (5), 389–399. doi:10.1016/j.radmeas.2012.02.013

AUTHOR CONTRIBUTIONS

WY: Conceptualization, Methodology, Investigation, Data curation, Writing—original draft. XL: Investigation, Data curation, Visualization. TL: Investigation, Resources, Conceptualization. SW: Investigation, Resources, Data curation. YX: Investigation, Validation. BZ: Investigation, Validation. RZ: investigation. FY: Conceptualization, Supervision, Writing—review and editing. DZ: Investigation, Resources, Formal analysis. JG: Investigation, Data curation, Visualization. All authors have read and agreed to the published version of the manuscript.

FUNDING

This work was jointly supported by the National Natural Science Foundation of China (Grant Numbers: 42102289 and 4210020524) and the National Geological Survey Project (Grant Numbers: DD20190129 and DD20221677).

- Lang, X. Y., Lin, W. J., Liu, Z. M., Xing, L. X., and Wang, G. L. (2016). Hydrochemical Characteristics of Geothermal Water in the Guide Basin. *Earth Sci.* 41 (10), 1723–1734. doi:10.3799/dqkx.2016.509
- Li, H. Q., Zhang, S. S., Xie, M. Z., Ren, J. S., and Zhou, J. F. (2020). Tectonic System and its Geothermal Water Controlling in Zhangjiakou Area. *Coal Geology. China* 32 (05), 74–82.
- Moghaddam, M. M., Mirzaei, S., Nouraliee, J., and Porkhial, S. (2016). Integrated magnetic and gravity surveys for geothermal exploration in Central Iran. *Arabian J Geosci.* 9, 506.
- Moore, J. P., and Walsh, J. J. (2021). Quantitative Analysis of Cenozoic Faults and Fractures and Their Impact on Groundwater Flow in the Bedrock Aquifers of Ireland. *Hydrogeol. J.* 29, 2613–2632. doi:10.1007/s10040-021-02395-z
- Peng, C., Pan, B., Xue, L., and Liu, H. (2019). Geophysical Survey of Geothermal Energy Potential in the Liaoji Belt, Northeastern China. *Geotherm Energy* 7 (1), 14. doi:10.1186/s40517-019-0130-y
- Pinti, D. L., Castro, M. C., Lopez-Hernandez, A., Han, G., Shouakar-Stash, O., Hall, C. M., et al. (2017). Fluid Circulation and Reservoir Conditions of the Los Humeros Geothermal Field (LHGF), Mexico, as Revealed by a noble Gas Survey. *J. Volcanology Geothermal Res.* 333-334 (334), 104–115. doi:10.1016/j.jvolgeores.2017.01.015
- Qi, B. S., Feng, C. J., Tan, C. X., Zhang, P., and Meng, J. (2019). Application of comprehensive geophysical-drilling exploration to detect the buried North Boundary active Fault Belt of Yanqing-Fanshan Basin in Sangyuan Town, Beijing-Zhangjiakou area. *Geol. China* 46 (3), 468–481. doi:10.12029/gc20190303
- Rodriguez, F., Perez, N. M., and Melian, G. V. (2021). Exploration of Deep-Seated Geothermal Reservoirs in the Canary Islands by Means of Soil CO₂ Degassing Surveys. *Renew. Energ.* 164, 1017–1028. doi:10.1016/j.renene.2020.09.065
- Sena-Lozoya, E. B., González-Escobar, M., Gómez-Arias, E., González-Fernández, A., and Gómez-Ávila, M. (2020). Seismic Exploration Survey Northeast of the Tres Virgenes Geothermal Field, Baja California Sur, Mexico: A New Geothermal prospect. *Geothermics* 84, 101743. doi:10.1016/j.geothermics.2019.101743
- Vaselli, O., Higuera, P., Nisi, B., Maria Esbri, J., Cabassi, J., Martínez-Coronado, A., et al. (2013). Distribution of Gaseous Hg in the Mercury Mining District of Mt. Amiata (Central Italy): A Geochemical Survey Prior the Reclamation Project. *Environ. Res.* 125, 179–187. doi:10.1016/j.envres.2012.12.010
- Wan, T. F. (2011). *The Tectonics of China*. Beijing: Geology Press.
- Wang, J. Y., Xiong, L. P., and Pang, Z. H. (1993). *Low to Medium Convective Type Geothermal Systems*. Beijing: Scientific press.
- Wang, W. X., Zhao, N., Zhang, Y. N., Cao, S. P., and Li, G. K. (2015). Geochemical Anomalies of Soil Elements and Their Implications for Geothermal fields in the Tianjin Area. *Geology. Exploration* 51 (5), 932–938. doi:10.13712/j.cnki.dzykt.2015.05.013

- Wang, G. L., Zhang, W., Liang, J. Y., Lin, W. J., Liu, Z. M., and Wang, W. L. (2017). Evaluation of Geothermal Resources Potential in China. *Acta Geoscientica Sinica* 38 (4), 449–459. doi:10.3975/cagsb.2017.04.02
- Wei, H. Z. (2006). A Discussion on Geothermal Resources in Zhangjiakou. *Coal Geology, China* 4, 38–41. doi:10.3969/j.issn.1674-1803.2006.04.015
- Xiao, N. S. (1986). *Analysis of Neotectonics and its Application in Groundwater Exploration*. Beijing: Geology Press.
- Yang, F. T., Pang, Z. H., Wang, C. H., Duan, Z. F., Luo, L., and Li, Y. M. (2012). Genesis Model of Laozishan Geothermal Field in the Subei Basin. *J. Jilin Univ. (Earth Sci. Edition)* 42 (2), 468–475. doi:10.3969/j.issn.1671-5888.2012.02.022
- Yuan, W. Z., Zhang, D. L., Xing, Y. F., Gao, J., Zhang, B. J., Li, Y. Y., et al. (2021). *Investigation and Evaluation Report of Geothermal Resources in Zhangjiakou Area*. Beijing: CGS.
- Zarroca, M., Linares, R., Bach, J., Roqué, C., Moreno, V., Font, L., et al. (2012). Integrated Geophysics and Soil Gas Profiles as a Tool to Characterize Active Faults: the Amer Fault Example (Pyrenees, NE Spain). *Environ. Earth Sci.* 67 (3), 889–910. doi:10.1007/s12665-012-1537-y

Conflict of Interest: The authors declare that the research was conducted in the absence of any commercial or financial relationships that could be construed as a potential conflict of interest.

Publisher's Note: All claims expressed in this article are solely those of the authors and do not necessarily represent those of their affiliated organizations or those of the publisher, the editors, and the reviewers. Any product that may be evaluated in this article, or claim that may be made by its manufacturer, is not guaranteed or endorsed by the publisher.

Copyright © 2022 Yuan, Lei, Liu, Wang, Xing, Zhu, Yang, Zhang, Gao and Zhang. This is an open-access article distributed under the terms of the Creative Commons Attribution License (CC BY). The use, distribution or reproduction in other forums is permitted, provided the original author(s) and the copyright owner(s) are credited and that the original publication in this journal is cited, in accordance with accepted academic practice. No use, distribution or reproduction is permitted which does not comply with these terms.